John von Neumann Institute for Computing

Transition to Turbulence in Magnetohydrodynamic Channel Flow of Liquid Metals

Egbert Zienicke, Thomas Boeck, and Dmitry Krasnov

published in

NIC Symposium 2006 ,
G. Münster, D. Wolf, M. Kremer (Editors),
John von Neumann Institute for Computing, Jülich,
NIC Series, Vol. **32**, ISBN 3-00-017351-X, pp. 341-348, 2006.

http://www.fz-juelich.de/nic-series/volume32

Transition to Turbulence in Magnetohydrodynamic Channel Flow of Liquid Metals

Egbert Zienicke[1], **Thomas Boeck**[2], **and Dmitry Krasnov**[2]

[1] Institut für Physik
Technische Universität Ilmenau, 98684 Ilmenau, Germany
E-mail: egbert.zienicke@tu-ilmenau.de

[2] Fakultät für Maschinenbau
Technische Universität Ilmenau, 98684 Ilmenau, Germany
E-mail: {thomas.boeck, dmitry.krasnov}@tu-ilmenau.de

A pseudospectral flow solver is implemented for the solution of the magnetohydrodynamic (MHD) equations in the quasistatic approximation which is valid for liquid metal flows in experimental and industrial setups. The code is based on a poloidal-toroidal decomposition of the velocity field and well suited for parallelization. Only the transposition of coefficient matrices needed in the Fast Fourier Transformation requires a higher amount of communication between processors. The MHD solver is applied to the problem of transition to turbulence in MHD channel flow. The streak breakdown scenario is investigated numerically for different Reynolds and Hartmann numbers to clear up the details of the transition process and to compare the numerically found critical Reynolds numbers with experimental values. A very good agreement is found.

1 Introduction

The goal of our project is to study wall bounded flow of an electrically conducting fluid under the influence of an external magnetic field. The motivation for these studies are industrial processes where electromagnetic processing of materials (EPM) is applied. This is very useful for casting of liquid metals as well as for growing of semiconductor crystals. The hot melt can be influenced by externally applied magnetic fields. An example is the electromagnetic brake, consisting of a strong, inhomogeneous, external magnetic DC field, that is used to brake the flow of a liquid metal melt. It is widely used in the process of continuous casting of steel. The braking prevents an inclusion of slag from the free surface and also limits the transport of the hot molten steel downward the already cooled slab. For an optimization of the product of the casting process the influence of the magnetic field on the melt flow has to be well understood. Therefore, we have first concentrated on the investigation of the transition to MHD turbulence and of MHD turbulence itself in wall bounded flows. The simplest geometry, for which this is possible, is an infinite slab bounded by a lower and an upper wall. A vertical, homogenous magnetic field is applied normal to the walls. The laminar pressure driven flow in this configuration is known as *Hartmann flow*[1]. The braking effect of the Lorentz force is created by induced currents in the fluid interacting with the external magnetic field. As a result one observes a flat profile in the middle of the channel and two Hartmann layers at the walls, in which current loops are closed and the main velocity gradient is located. The thickness δ of the Hartmann

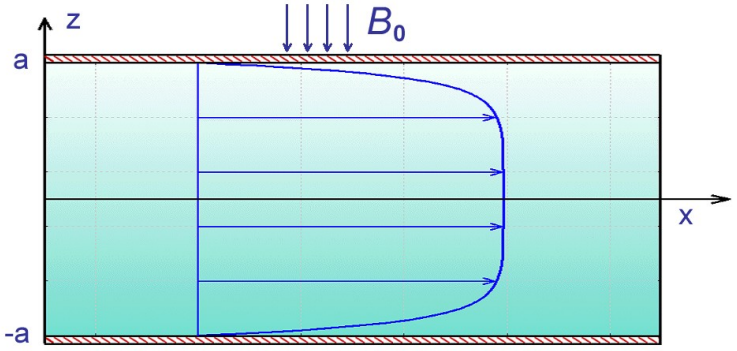

Figure 1. Schematic picture of channel geometry.

layers is determined by the dimensionless Hartmann number Ha:

$$\delta = \frac{a}{Ha} \qquad \text{with} \qquad Ha = B_0 a \sqrt{\frac{\sigma}{\rho\nu}}, \tag{1}$$

where a is the channel half-width, B_0 the imposed magnetic field, σ the electric conductivity, ρ the density and ν the kinematic viscosity. The Hartmann number gives a dimensionless measure of the ratio between the Lorentz force and viscous forces in the flow. For the discussion of the transition to turbulence in section 3 we also introduce the Reynolds number $R = U\delta/\nu$ based on the Hartmann layer thickness and the centerline velocity U.

2 Governing Equations and Code Description

The basic equations are the incompressible Navier-Stokes equations

$$\rho\left(\frac{\partial \boldsymbol{v}}{\partial t} + (\boldsymbol{v}\cdot\nabla)\boldsymbol{v}\right) = -\nabla p + \rho\nu\nabla^2\boldsymbol{v} + \boldsymbol{j}\times\boldsymbol{B}_0, \tag{2}$$

$$\nabla\cdot\boldsymbol{v} = 0, \tag{3}$$

for the velocity field $\boldsymbol{v}$ including the Lorentz force term $\boldsymbol{j}\times\boldsymbol{B}_0$, where $\boldsymbol{B}_0$ denotes the external magnetic field. The induced current $\boldsymbol{j}$ giving rise to the Lorentz force is computed in the quasistatic approximation[2] for low magnetic Reynolds numbers, which is appropriate for the flows found in the laboratory and industrial facilities. It is given by Ohm's law

$$\boldsymbol{j} = \sigma\left(-\nabla\phi + \boldsymbol{v}\times\boldsymbol{B}_0\right), \tag{4}$$

where we have introduced the electric potential ϕ and the conductivity σ. The electric potential is found from the condition

$$\nabla\cdot\boldsymbol{j} = 0 \Rightarrow \nabla^2\phi = \nabla\cdot\left(\boldsymbol{v}\times\boldsymbol{B}_0\right). \tag{5}$$

The boundary condition for the velocity on the channel walls is the no-slip condition $\boldsymbol{v} = 0$. For electrically insulating channel walls the normal component j_n of the electric current

vanishes. This provides the boundary conditions for the Poisson equation of the electric potential.

Our pseudospectral code is based on the so-called poloidal-toroidal representation of the velocity field as

$$\boldsymbol{v}(x,y,z,t) = \boldsymbol{\nabla} \times (\boldsymbol{\nabla} \times \boldsymbol{e}_z \varphi(x,y,z,t)) + \boldsymbol{\nabla} \times \boldsymbol{e}_z \psi(x,y,z,t). \tag{6}$$

This decomposition satisfies the incompressibility condition $\nabla \cdot \boldsymbol{v} = 0$ automatically, and we can therefore eliminate the pressure when we substitute (6) into the Navier-Stokes equations. The evolution equations for the velocity potentials φ and ψ and the electric potential ϕ are of the form

$$\mathcal{M}\partial_t f = \mathcal{L}f + \mathcal{N}(\phi, \psi, \varphi), \tag{7}$$

where $\mathcal{L}$ and $\mathcal{M}$ are linear (spatial) operators, $\mathcal{N}$ is the nonlinearity, and the variable f denotes one of the three variables φ, ψ, ϕ.

Our computational domain is periodic in the horizontal directions x and y with periodicity intervals L_x and L_y. We expand every quantity in a double Fourier series with respect to those coordinates and the basic wave numbers $k_x = 2\pi/L_x$ and $k_y = 2\pi/L_y$. With respect to the vertical direction, Chebyshev polynomials T_p are used (p denotes the order of the polynomial and $2a$ the channel width), i.e.

$$f(x,y,z,t) = \sum_{r=-N_x/2}^{N_x/2-1} \sum_{s=-N_y/2}^{N_y/2-1} \sum_{p=0}^{N_z} \mathrm{e}^{irk_x x + isk_y y}\, T_p(z/a)\, \hat{f}^{(r,s,p)}(t). \tag{8}$$

The numbers N_x and N_y denote the number of Fourier modes with respect to the x and y direction, N_z stands for the number of Chebyshev polynomials and $\hat{f}^{(r,s,p)}(t)$ for the time-dependent expansion coefficients. Upon substitution of the expansions (8) into the partial differential equations (7) we obtain a system of coupled ordinary differential equations for the coefficients $\hat{f}^{(r,s,p)}(t)$. The linear operators $\mathcal{L}$ and $\mathcal{M}$ couple only the expansion coefficients for the same wave numbers rk_x and sk_y. For this reason, we can treat the different wave numbers separately in what follows. The expansion coefficients $\hat{f}^{(r,s,p)}(t)$ with the same r and s are written as a column vector $\hat{\boldsymbol{f}}_{r,s}$ with dimension $N_z + 1$. The systems of differential equations for each set of (r, s) are therefore

$$\boldsymbol{\mathcal{M}}_{r,s}\partial_t \hat{\boldsymbol{f}}_{r,s} = \boldsymbol{\mathcal{L}}_{r,s}\hat{\boldsymbol{f}}_{r,s} + \boldsymbol{\mathcal{N}}_{\boldsymbol{r,s}}(\phi, \psi, \varphi), \tag{9}$$

where we have introduced the indices (r, s) on the linear and nonlinear operators. The nonlinear term $\mathcal{N}$ couples expansion coefficients for different wave numbers and acts therefore not only on $\hat{\boldsymbol{f}}_{r,s}$. To solve the time-evolution problem we apply a finite-difference method with time step Δt. It can be denoted as

$$\begin{aligned} \boldsymbol{\mathcal{M}}_{r,s}\frac{3\hat{\boldsymbol{f}}^{n+1}_{r,s} - 4\hat{\boldsymbol{f}}^{n}_{r,s} + \hat{\boldsymbol{f}}^{n-1}_{r,s}}{2\Delta t} &= \boldsymbol{\mathcal{L}}_{r,s}\hat{\boldsymbol{f}}^{n+1}_{r,s} \\ +2\boldsymbol{\mathcal{N}}_{r,s}(\phi^n, \psi^n, \varphi^n) - \boldsymbol{\mathcal{N}}_{r,s}(\phi^{n-1}, \psi^{n-1}, \varphi^{n-1}). & \end{aligned} \tag{10}$$

The left hand side approximates the time derivative at the time level $n+1$ using the previous two time levels. The nonlinear term is treated using the second-order Adams-Bashforth method, where the prefactors correspond to a linear extrapolation to the time level $n + 1$.

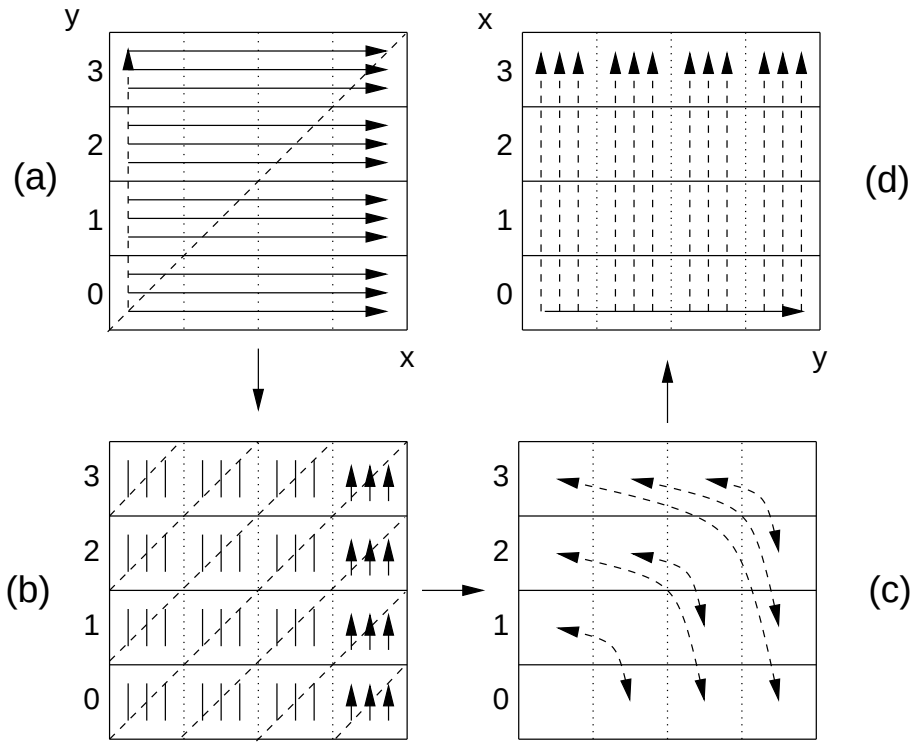

Figure 2. Data array transposition across processes for parallelized FFT. Initial distribution of data is indicated by the full arrows in (a), where the frame boxes correspond to the individual processes numbered from 0 to 3. The dashed arrow indicates that one-dimensional transforms in y direction cannot be computed this way. To remedy this problem, a transposition about the diagonal (shown as dashed line) is necessary. It proceeds by local sub-array transposition (b) and swapping sub-arrays between processes (c) in order to arrive at the desired distribution (d).

This method is second-order accurate in the time step Δt. To find $\hat{\boldsymbol{f}}_{r,s}^{n+1}$ we only have to solve a system of linear equations of dimension $N_z + 1$ with a banded structure.

Most of the computational time is spent on the nonlinear terms $\mathcal{N}$. A direct evaluation of these terms in the spectral representation is neither simple nor computationally efficient. They are therefore calculated in physical space using inverse Fourier transforms, which provide us the values of the variable ϕ, ψ and φ at certain collocation points from the expansion coefficients. Direct Fourier transforms are then used to calculate the expansion coefficients of $\mathcal{N}$ from its values at these collocation points[3].

The parallelization of the numerical algorithm can be accomplished by domain decomposition with respect to the x or y direction. Only the Fourier transforms will then require inter-process communication. In our implementation, the transform proceeds as a successive application of one-dimensional transforms with respect to x, y and z. The transform for the divided direction is avoided by a transposition of the data array containing the expansion coefficients, which is explained in Fig. 2. The transposition requires fast inter-process communication and therefore benefits greatly from using the high-end parallel computers at the NIC.

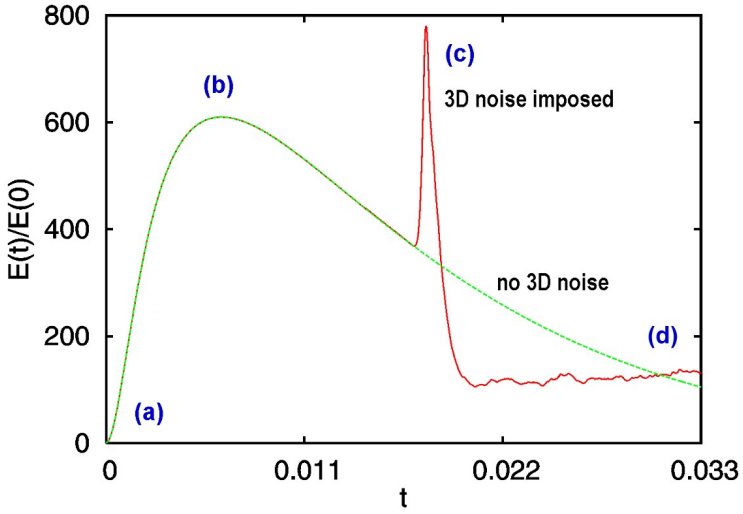

Figure 3. Evolution of the energy of the perturbation from the basic flow profile. The green curve shows the 2D evolution in which the nonlinearity of the Navier-Stokes equation is suppressed. After reaching the maximum the perturbation decays exponentially corresponding to stability of the linear system. A small random 3D perturbation applied at the maximum of the perturbation (marked by (b)) grows exponentially for full 3D evolution of the system and at a certain point the transition to turbulence begins marked by a sharp spike of the perturbation (red curve).

3 Transition by the Streak Breakdown Mechanism

With the pseudospectral code the transition to turbulence in the Hartmann flow was investigated[4,5]. From several experiments it was clear that the linear instability threshold of the Hartmann profile, located at a Reynolds number of $R_c = 48250$ cannot be responsible for the transition to turbulence[6]. The transition was found to be in the range $150 \leq R_c \leq 250$ in the older experiments[7,8] and localized more precisely in a recent experiment[9] at $R_c \approx 380$. Our hypothesis was that the transition to turbulence in this system takes place by the streak breakdown scenario which is one of the possible bypass scenarios proposed for several shear flows in the last decade[10]. The common feature of these scenarios is that they all involve two steps, where the first depends on finite-sized perturbations explaining the fact that one cannot identify a unique critical Reynolds number. Instead, the transition takes place in a whole range of Reynolds numbers.

The streak breakdown scenario, which we tested numerically on the Hartmann flow, takes place in the following way: In a first step we have applied so called optimal disturbances[10] to the basic flow. Optimal disturbances are stable for the linearized Navier-Stokes equation, but they can have a very strong initial growth after which they decay exponentially. The maximum amplification depends on the Reynolds number and can easily attain a value of 2000 measured in units of the initial perturbation energy. For our system the optimal disturbances are streamwise vortices which are located in the Hartmann layer and whose wavelength is of the order of the thickness of the Hartmann layers. To suppress the nonlinearity of the Navier-Stokes equation we forced the flow to stay on a two-dimensional

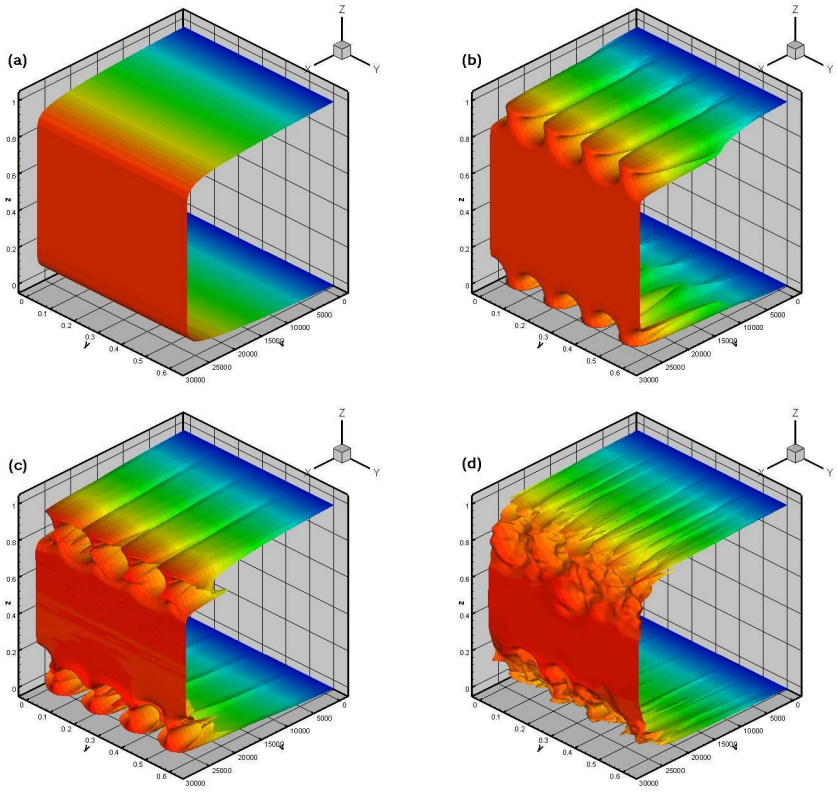

Figure 4. Flow profiles in a plane $x = const$ for four chosen time moments of the streak breakdown scenario at Reynolds number $R = 500$ and Hartmann number $Ha = 40$. (a) Initial condition consisting of laminar Hartmann flow plus 2D-optimal disturbance. The latter is so small that the perturbation is not visible in the profile. (b) After time evolution in two dimensions the 2D-disturbance has reached its maximum energy. The streaks at both boundaries can be clearly seen. (c) After the application of the 3D-perturbation the computation of the time evolution is fully three-dimensional. Here the streak breakdown begins starting the transition to turbulence. (d) The turbulent state has been reached.

evolution by suppressing all Fourier modes belonging to a spacial dependence in streamwise direction. This growth phase can be seen in figure 3 showing the energy evolution of the perturbation. With (a) the initial condition is marked, whose velocity profile can be seen in plot (a) of figure 4. The perturbation of the Hartmann profile in the initial state is too small to be visible. With the growth of the optimal perturbations streamwise streaks in the flow evolve which are characterized by alternating stripes of low and high velocity in spanwise direction (see flow profile (b) of figure 4). If the 2D evolution, suppressing the nonlinearity of the Navier-Stokes equation, is pursued further the energy of the perturbation decays exponentially. This corresponds to the fact that the Hartmann flow is linearly stable.

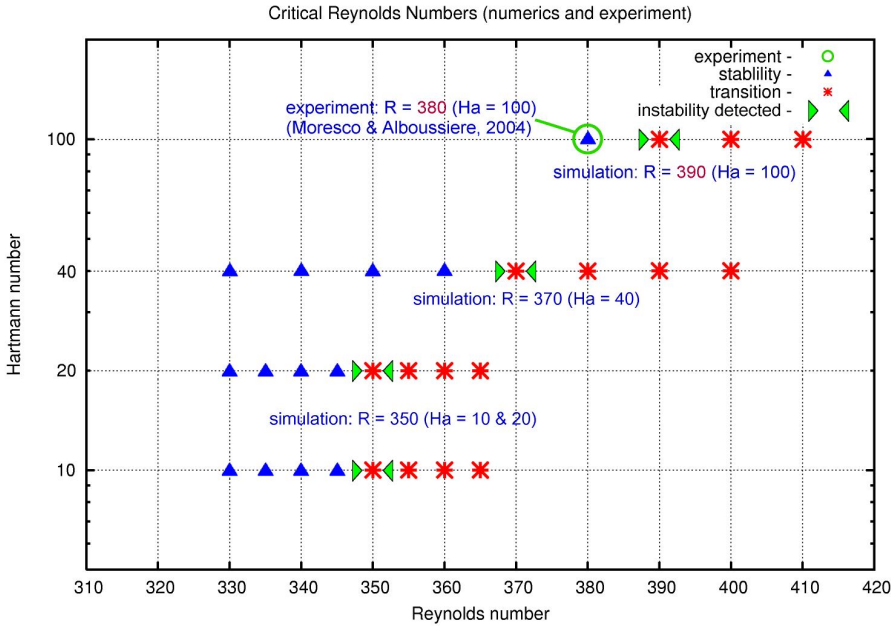

Figure 5. Critical Reynolds number R vs Hartmann number. Filled triangles mark points (R, Ha) in the parameter space, where no transition could be detected independent on the size of 2D- and 3D-perturbations. Empty triangles mark parameter pairs, where a transition by the streak breakdown scenario could be observed. The numerical value of the critical Reynolds number approaches the experimental value for $Ha = 40$ and 100 giving a better agreement with reference[9].

At the time of the maximum ampification of the optimal perturbation a random 3D perturbation is added and the full 3D evolution of the system is switched on in the flow solver. This constitutes the second step of the streak breakdown scenario and allows the nonlinearity of the Navier-Stokes equation to act on the flow which is unstable against small 3D perturbations. Plot (c) of figure 3 shows the profile directly after the application of the 3D random perturbation, and plot (d) is a snapshot of the turbulent state which is reached after the transition phase.

So far, it has been shown that the streak breakdown mechanism is able to trigger transition to turbulence for the Hartmann flow. We find critical Reynolds numbers for the transition that are very close to the experiment of Moresco & Alboussière[9]. We interpret this as a strong indication that the streak breakdown scenario really describes the physics of the transition to turbulence in our system. However, the experiments were carried out in a Hartmann number range between 130 and 1690, which extends to much higher values than our numerical calculations. To close the gap between the Hartmann numbers of our numerical simulations and the experiment we performed a systematic check of stability and instability dependent on Reynolds number R and Hartmann number Ha. This is shown in Figure 5. The black filled triangles denote that for the corresponding R and Ha no transition to turbulence was observed with the two-step scenario, irrespective of how large the 2D-optimal disturbances and 3D-random perturbations were chosen. Blank

triangles mark the runs, where a transition to turbulence could be found with the two-step mechanism with a certain choice of 2D- and 3D-perturbations. The runs for $Ha = 10$ and 20, which were first presented in[4], all yield a critical Reynolds number in the interval $345 < R_c < 350$, which is already very close to the experimental value of $R_c = 380$ found by Moresco & Alboussière. In our recent paper 5 computations for the higher Hartmann numbers $Ha = 40$ and 100 are presented leading to slightly higher values $360 < R_c < 370$ and $380 < R_c < 390$, respectively, for the critical Reynolds number. This is closer to the result of the experiment and closes the gap between numerics and experiment well. As the critical Reynolds number still varies with the Hartmann number the numerical calculations show that the limit of an isolated Hartmann layer is not yet reached for $Ha = 40$ and $Ha = 100$. Because one needs several runs to bracket the critical Reynolds number for a given Hartmann number, it was not possible to treat the case of higher Hartmann numbers (the next would have been $Ha = 200$) with our computational resources.

Acknowledgements

The authors are grateful for financial support of the Deutsche Forschungsgemeinschaft in the framework of the Research Group Magnetofluiddynamics and through an Emmy Noether fellowship (Bo 1668/2-2). Most of the numerical simulations were performed on the computers at the John von Neumann - Institut für Computing.

References

1. J. Hartmann. Hg-dynamics i: Theory of the laminar flow of an electrically conductive liquid in a homogeneous magnetic field. *K. Dan. Vidensk. Selsk. Mat. Fys. Medd.*, 15(6):1–28, 1937.
2. P. A. Davidson. *An Introduction to Magnetohydrodynamics*. Cambridge University Press, 2001.
3. C. Canuto, M. Y. Hussaini, A. Quateroni, T. A. Zang. *Spectral Methods in Fluid Dynamics*. Springer Verlag, 1988.
4. D. S. Krasnov, E. Zienicke, O. Zikanov, T. Boeck, and A. Thess. Numerical study of instability and transition to turbulence in the Hartmann flow. *J. Fluid Mech*, 504:183–211, 2004.
5. E. A. Zienicke, D. S. Krasnov. Parametric study of streak breakdown mechanism in Hartmann flow *Phys. Fluids*, 17:114101, 2005.
6. R. J. Lingwood and T. Alboussiere. On the stability of the Hartmann layer. *Phys. Fluids*, 11:2058–2068, 1999.
7. W. Murgatroyd. Experiments on magnetohydrodynamic channel flow. *Philos. Mag.*, 44:1348–1354, 1953.
8. G. Branover and A. Tsinober. *Magnetohydrodynamics of incompressible fluids*. Nauka, Fys.Mat.Lit., 1970.
9. P. Moresco and T. Alboussiere. Experimental study of the instability of the Hartmann layer. *J. Fluid Mech*, 504:167–181, 2004.
10. P. J. Schmid and D. S Henningson. *Stability and Transition in Shear Flows*. Springer Verlag, 2001.